A Mathematical Model of Alveolar Gas Exchange in Partial Liquid Ventilation

Vinod Suresh

Joseph C. Anderson

James B. Grotberg

Department of Biomedical Engineering,
University of Michigan, Ann Arbor, MI 48109

Ronald B. Hirschl

Department of Surgery, University of Michigan,
Ann Arbor, MI 48109

In partial liquid ventilation (PLV), perfluorocarbon (PFC) acts as a diffusion barrier to gas transport in the alveolar space since the diffusivities of oxygen and carbon dioxide in this medium are four orders of magnitude lower than in air. Therefore convection in the PFC layer resulting from the oscillatory motions of the alveolar sac during ventilation can significantly affect gas transport. For example, a typical value of the Péclet number in air ventilation is Pe~0.01, whereas in PLV it is Pe~20. To study the importance of convection, a single terminal alveolar sac is modeled as an oscillating spherical shell with gas, PFC, tissue and capillary blood compartments. Differential equations describing mass conservation within each compartment are derived and solved to obtain time periodic partial pressures. Significant partial pressure gradients in the PFC layer and partial pressure differences between the capillary and gas compartments (P_C-P_g) are found to exist. Because Pe≫1, temporal phase differences are found to exist between P_C-P_g and the ventilatory cycle that cannot be adequately described by existing nonconvective models of gas exchange in PLV. The mass transfer rate is nearly constant throughout the breath when Pe≫1, but when Pe≪1 nearly 100% of the transport occurs during inspiration. A range of respiratory rates (RR), including those relevant to high frequency oscillation (HFO)+PLV, tidal volumes (V_T) and perfusion rates are studied to determine the effect of heterogeneous distributions of ventilation and perfusion on gas exchange. The largest changes in $P_C O_2$ and $P_C CO_2$ occur at normal and low perfusion rates respectively as RR and V_T are varied. At a given ventilation rate, a low RR-high V_T combination results in higher $P_C O_2$, lower $P_C CO_2$ and lower (P_C-P_g) than a high RR-low V_T one. [DOI: 10.1115/1.1835352]

Keywords: Partial Liquid Ventilation, Liquid Breathing, Perfluorocarbon, Gas Exchange, Convection

1 Introduction

Liquid breathing in mammals using perfluorocarbon (PFC) was first demonstrated by Clark and Gollan [1]. Since then the concept has led to the development of partial liquid ventilation (PLV) as a promising alternative to conventional mechanical gas ventilation (GV) for treating acute respiratory distress syndrome (ARDS) and acute lung injury (ALI). Studies on animal models [2–6] and human trials [7–11] have indicated improvement in gas exchange and lung compliance associated with the use of PLV.

Recent studies have examined the effects of PLV on regional ventilation ($\dot{V}_A$) and blood flow ($\dot{Q}$) distribution in the lung in order to understand the mechanisms behind the global changes in gas exchange and lung mechanics. PFC was found to be predominantly distributed in the dependent regions of injured adult sheep lungs undergoing PLV and more gas than PFC was found to be present in the nondependent regions of the lung [6]. Redistribution of blood flow from the dependent to the nondependent regions of the lung was observed during PLV in lambs [12] and pigs [13]. Ventilation-perfusion ($\dot{V}_A/\dot{Q}$) inhomogeneity was found to be higher during PLV compared to GV in healthy piglets [14]. Significant regions with low $\dot{V}_A/\dot{Q}$ ratios were observed in rabbits with acute lung injury during PLV [15]. Harris et al. [16] compared regional distributions of ventilation, blood flow, and ventilation-perfusion ratio in the normal lung of a sheep during PLV and GV. They found that both ventilation and perfusion are shifted from the dependent regions to the nondependent regions of

the lung in PLV, leading to a wide distribution of $\dot{V}_A/\dot{Q}$ in different regions of the lung. In contrast $\dot{V}_A/\dot{Q}$ ratios were close to unity over most of the lung in GV. In order to understand the mechanisms responsible for improved gas exchange in PLV, it is crucial to determine the contribution to gas exchange of regions whose $\dot{V}_A$, $\dot{Q}$, and $\dot{V}_A/\dot{Q}$ differ significantly from their normal values in GV.

Previous animal studies indicated enhanced arterial-alveolar (a-A) partial pressure gradients in PLV as a result of increased shunt fraction and ventilation-perfusion heterogeneity [14]. Van-Löbensels et al. developed a mathematical model of gas exchange during PLV in lung subunits with a PFC layer that indicated a diffusion limitation could lead to significant (a-A) gradients [17]. However they only considered diffusion of respiratory gases through a stagnant layer of PFC in an alveolar sac. In reality the expansion and contraction of the sac during tidal ventilation creates a flow field within the PFC layer contained inside. The importance of convective effects on transport can be estimated through the Péclet number, Pe$= 2\pi f R^2/D$, where f is the breathing frequency in breaths/second, R is the sac radius, and D is the gas diffusivity in the alveolar medium (air in GV, PFC, in PLV). Values of Pe≫1 indicate that convection plays a significant role in transport while values of Pe≪1 indicate that diffusion is the dominant transport mechanism. At normal respiratory rates, Pe $\sim 10^{-3} - 10^{-2}$ in GV while it is on the order of 15–50 in PLV. This is a result of the small diffusivities of O_2 and CO_2 in PFC, which are 1000–10,000 times smaller than in air. Thus convective effects play an important role in the transport of respiratory gases
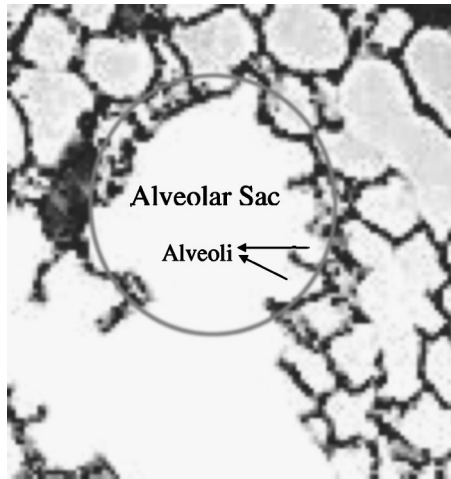
Fig. 1 Micrograph of mammalian lung parenchyma (200×) showing alveolar sac and associated alveoli (courtesy of Professor Rick Gillis, Department of Biology University of Wisconsin-La Crosse)

Fig. 2 Schematic of the alveolar sac model. An oscillating spherical shell of radius $R_S(t)$ encapsulated by a tissue layer of thickness h represents the sac. A well-mixed capillary blood compartment perfused at a constant blood flow rate $\dot{Q}$ surrounds the sac. A well-mixed central core of radius $R_g(t)$ inside the sac supplies fresh gas at a constant partial pressure P_{in} during inspiration and removes expired gas at partial pressure $P_g(t)$ during expiration.

through the PFC layer. In this work we extend the model of Van-Löbensels et al. to include the effects of the PFC flow field on gas transport.

A given ventilation rate $\dot{V}_A$ may be obtained using different combinations of respiratory rates (RR) and tidal volumes (V_T) since $\dot{V}_A = \text{RR} \times V_T$. Our model allows the specification of both RR and V_T independently in contrast to the model of Van-Löbensels et al. in which only $\dot{V}_A$ could be specified. As a result the effect of both tidal volume and respiratory rate on gas exchange can be determined. This difference is especially important from a clinical perspective since ventilation strategies for choosing RR and V_T are usually aimed at meeting target blood gas tensions. However studies have indicated that the use of large tidal volumes coupled with large PFC doses increases the risk of alveolar rupture [18]. Therefore there has been interest in developing effective "lung-protective" ventilation strategies to minimize the risk of ventilator-induced lung injury. One such strategy involving the combination of high frequency oscillation (HFO) with PLV (HFO+PLV) has been found to enhance lung protection while providing adequate gas exchange [19–23]. These studies have shown that, in general, gas exchange is not improved compared to PLV with conventional ventilation. The current work aims at providing an understanding of the physical transport mechanisms in lung subunits partially filled with PFC and their dependence on tidal volumes and respiratory rates, which can help explain the observations of experimental studies and provide guidance in developing optimal ventilation strategies.

2 Model

2.1 Description of the Model. Following VanLöbensels et al. [17] we model functional subunits of the lung at the level of alveolar sacs that comprise of several alveoli opening into a common chamber as shown in Fig. 1. The shape of these sacs is irregular and varies widely within the lung, but the overall size is fairly constant [24]. In order to reduce the geometrical complexity, we replace the asymmetric sacs with spherical structures of the same mean size, marked by the circle in Fig. 1. The simplified model is shown in Fig. 2, in which a terminal alveolar sac is modeled as an oscillating spherical shell with internal radius $R_S(t)$ at time t, encapsulated by a tissue layer of thickness h. This layer represents the respiratory membrane and is assumed to be much thinner than the radius of the sac $[h \ll R_S(t)]$. The interior of the shell consists of two regions: (1) A well-mixed central gas core with radius $R_g(t)$; (2) a shell of PFC between the core and
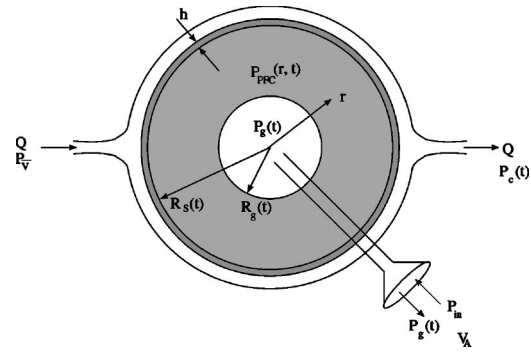
the alveolar wall in which liquid flow is driven by ventilation of the sac. In the course of ventilation, tidal volumes of gas enter and leave the sac through the core. A well-mixed capillary blood compartment perfused by a constant blood flow rate $\dot{Q}$ surrounds the shell. Blood enters the compartment with constant mixed venous gas partial pressures $P_{\bar{V}}$ and exits with capillary pressures $P_C(t)$.

Over the course of a breath, O_2 and CO_2 transport occurs between the gas core and the tissue–blood interface. In normal air breathing, the sac is completely filled with air and the dominant transport mechanism is diffusion. During PLV, the sac is partially liquid-filled and tidal ventilation results in liquid flow within the PFC layer. Since diffusion is about 4 orders of magnitude slower in PFC compared to air, this flow plays an important role in the transport of O_2 and CO_2. In the following sections, we will derive and solve equations for gas transport that incorporate the effect of flow in the PFC layer.

The spherical model used here is a highly simplified description of the actual asymmetric geometry of alveolar sacs. In order to justify the simplification, we note that gas exchange at the level of alveolar sacs averages contributions from many alveoli. Therefore we expect the results to be less sensitive to geometrical details and depend primarily on gross geometrical features such as the volume and surface area of the sac, which are fixed by choosing the diameter of the spherical model to match the average size of adult human alveolar sacs measured from micrographs, as explained in Sec. 2.3. With this choice of dimensions the model reproduces well-established experimental results for normal air breathing (Sec. 3.1), which provides support to the assumptions.

2.2 Governing Equations. The sac expands and contracts as a result of ventilation during the course of a breathing cycle. The variation of the sac radius with time is modeled by choosing a sinusoidal breathing pattern with an $I{:}E$ ratio of 1:2 as shown in Fig. 3. Thus

$$R_S(t) = R_{\text{FRC}}[1 + \delta f(t)], \tag{1}$$

where R_{FRC} is the minimum radius of the sac when the lung volume is equal to the functional residual capacity (FRC) and

$$f(t) = \begin{cases} \dfrac{1 - \cos(3\omega t/2)}{2}, & 0 < t < 2\pi/3\omega \\[2ex] \dfrac{1 - \cos(3\omega t/4 + \pi/2)}{2}, & 2\pi/3\omega \leq t \leq 2\pi/\omega. \end{cases} \tag{2}$$

The breathing frequency $\omega = 2\pi \text{RR}/60$ where RR is the respiratory rate in breaths per minute. At end-expiration $(t=0)$ $f(t)=0$,
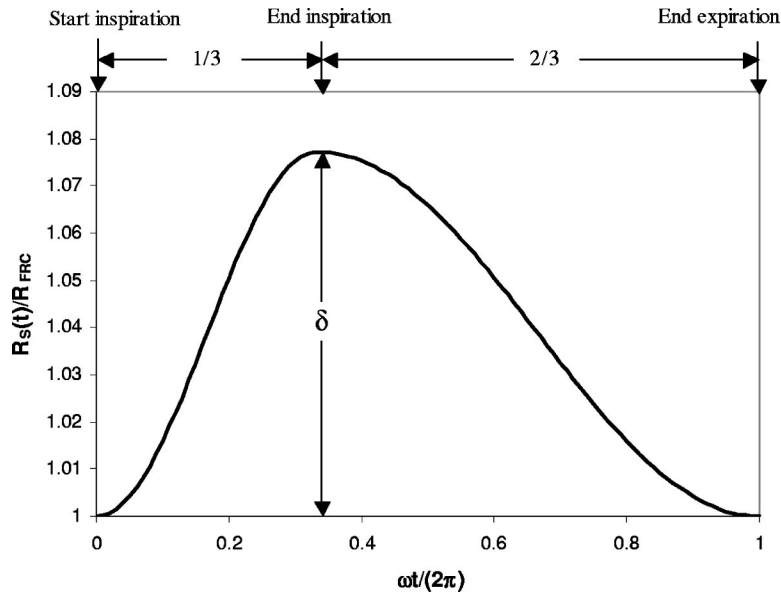
Fig. 3 Waveform of the duty cycle with $I:E=1:2$ over one breath. Time is normalized with the breathing period, $2\pi/\omega$, and the sac radius with the minimum radius, R_{FRC}. The maximum radius is equal to $R_{\text{FRC}}(1+\delta)$ and occurs at end inspiration.

$R_S(t) = R_{\text{FRC}}$ and at end-inspiration $(t = 2\pi/3\omega)\ f(t) = 1$, $R_S(t) = R_{\text{FRC}}(1+\delta)$. Assuming that the tidal volume V_T is equally divided among N_S sacs, δ is determined from the relation

$$(4\pi/3)R_{\text{FRC}}^3(1+\delta)^3 - (4\pi/3)R_{\text{FRC}}^3 = V_T/N_S. \tag{3}$$

Gas solubilities in air (β_g), PFC (β_{PFC}), and tissue (β_T) are constant, so gas concentrations C are converted to partial pressures P using the relation $C = \beta P$. However, gas solubilities in blood are nonlinear functions of P and are calculated from blood-gas dissociation relationships described later in this section. Gas transport in the model is described by coupled partial differential equations that relate the rate of change of partial pressure in each compartment to the delivery and removal of gas via ventilation, perfusion, convection and diffusion.

In the gas core, $P = P_g(t)$ and the rate of change of mass is balanced by the flow rate of gas into or out of the core due to ventilation and the diffusive flux at the core-PFC layer boundary:

$$\beta_g \frac{d}{dt}\left(\frac{4\pi}{3}R_g^3(t)P_g\right) = 4\pi R_g^2(t)\frac{dR_g}{dt}\beta_g P_0$$

$$+ 4\pi R_g^2(t)D_{\text{PFC}}\beta_{\text{PFC}}\frac{\partial P_{\text{PFC}}}{\partial r}\bigg|_{r=R_g(t)}. \tag{4}$$

Here, $R_g(t)$ is the radius of the gas core and D_{PFC} is the gas diffusivity in PFC. The first term on the right-hand side is equal to the gas flow rate into/out of the core during inspiration/expiration. During inspiration $P_0 = P_{\text{in}}$, the partial pressure of inspired gas. During expiration exhaled gas leaves the core with $P_0 = P_g(t)$. The volume of the sac, $V_S = 4\pi R_S^3(t)/3$, changes during the course of ventilation. Since the volume of PFC in the sac remains constant, the rate of change of core volume is equal to the rate of change of sac volume. Therefore,

$$R_g^2(t)\frac{dR_g}{dt} = R_S^2(t)\frac{dR_S}{dt}, \tag{5}$$

which yields the solution

$$R_g^3(t) - R_g^3(0) = R_S^3(t) - R_{\text{FRC}}^3. \tag{6}$$

The radius of the gas core at end expiration, $R_g(0)$, depends on the PFC dose. When $R_g(0)$ approaches R_{FRC} the model represents an air filled sac undergoing GV. When $R_g(0)$ approaches zero, the sac is completely filled with PFC.

The partial pressure $P_{\text{PFC}}(r,t)$ in the PFC layer is described by a convective-diffusive equation:

$$\frac{\partial P_{\text{PFC}}}{\partial t} + u_r(r,t)\frac{\partial P_{\text{PFC}}}{\partial r} = \frac{D_{\text{PFC}}}{r^2}\frac{\partial}{\partial r}\left(r^2\frac{\partial P_{\text{PFC}}}{\partial r}\right). \tag{7}$$

Table 1 Respiratory parameters for air breathing, conventional PLV, and HFO+PLV

	Air breathing	PLV	HFO+PLV
FRC (ml/kg)	34.1	30	30
V_T (ml/kg)	5	2.5–25	0.1–5
RR (breaths/min)	15	2.5–25	60–900
PFC dose (ml/kg)	⋯	25	25
$\dot{Q}$ (ml/min)	3.57×10^{-4}	3.57×10^{-5} 3.57×10^{-4} 3.57×10^{-3}	3.57×10^{-5} 3.57×10^{-4} 3.57×10^{-3}
$\dot{V}_A/\dot{Q}$	1.05	0.026–35	0.034–63

Table 2 Solubilities [ml gas/(100 ml solvent mm Hg)] and diffusivities (cm²/s) of O_2 and CO_2 in different media. Solubility of gas in air is defined to be 100/760 ml/(100 ml air mm Hg)

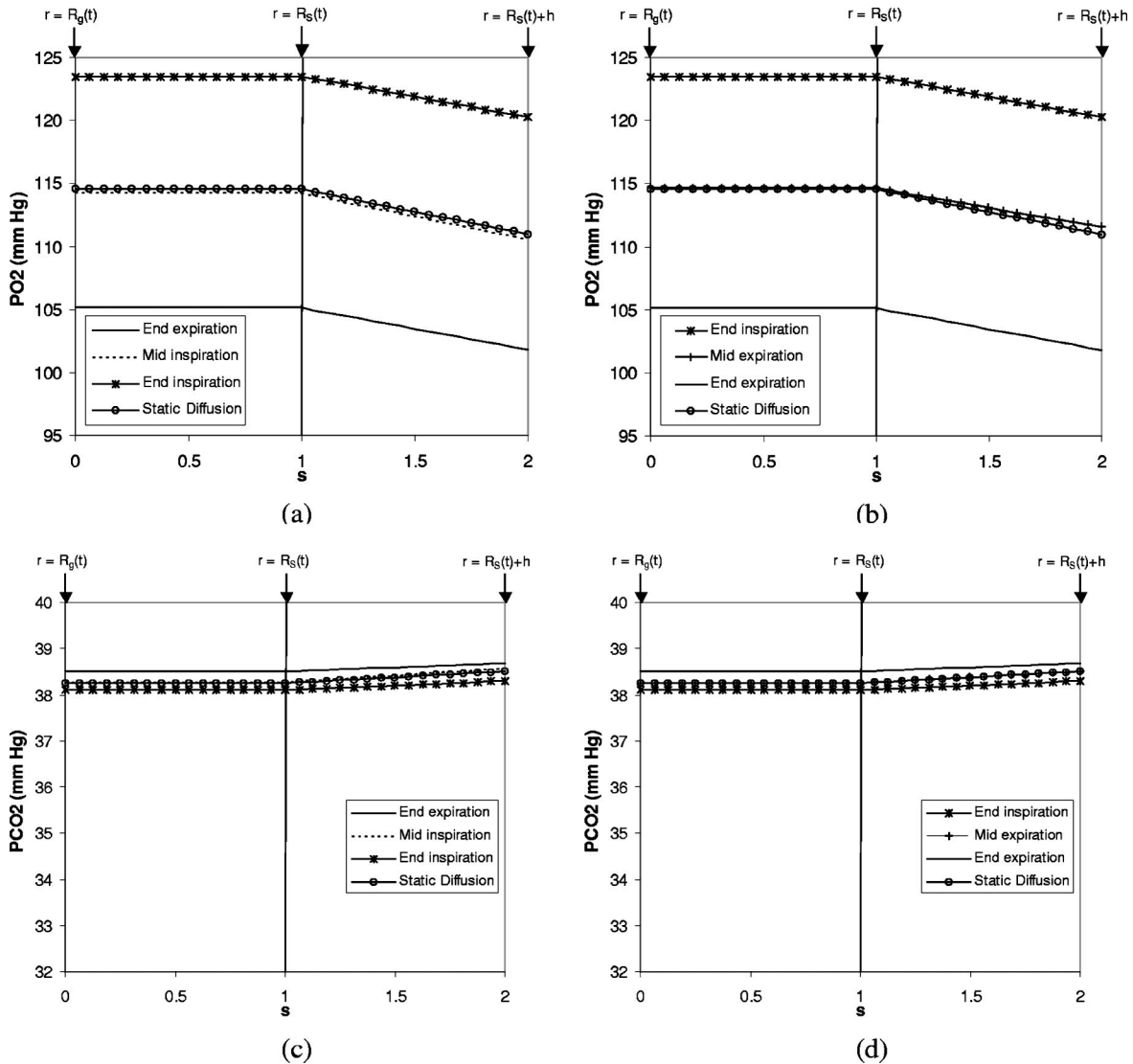|	O_2	CO_2
β_{air}	0.132	0.132
β_{PFC}	0.0656	0.256
β_T	0.003	0.057
β_P	0.003	0.057
D_{air}	0.190	0.147
D_{PFC}	5.61×10^{-5}	4.36×10^{-5}
D_T	1.2×10^{-5}	0.96×10^{-5}

Fig. 4 Partial pressure profiles during GV: (*a*) PO$_2$ during inspiration, (*b*) PO$_2$ during expiration, (*c*) *P*CO$_2$ during inspiration, (*d*) *P*CO$_2$ during expiration. Static diffusion profile is plotted for comparison. All profiles in the sac are flat because of the relatively high diffusivities of O$_2$ and CO$_2$ in air. Profiles are linear in the tissue layer; *s* is a normalized radial coordinate [see Eq. (21)]. The scale of the tissue layer is greatly exaggerated.

Ventilation of the sac drives a radial flow field within the PFC layer and results in convective gas transport within the layer, which is given by the second term in Eq. (7). The radial PFC velocity, $u_r(r,t)$, at a distance r from the center is determined by equating the rate of volume change, dV_S/dt, to the flow rate across a shell of surface area $4\pi r^2$. Thus,

$$4\pi r^2 u_r(r,t) = \frac{dV_S}{dt} = 4\pi R_S^2(t) \frac{dR_S}{dt}, \qquad (8)$$

which gives

$$u_r(r,t) = \frac{R_S^2(t)}{r^2} \frac{dR_S}{dt}. \qquad (9)$$

The third term in the equation describes diffusive gas transport in the PFC layer.

Since the thickness of the respiratory membrane is much smaller than the sac radius [$h \ll R_S(t)$], a thin-layer approximation is used in this region. As a result, convective transport and time derivative terms can be neglected and a diffusion equation is obtained:

$$\frac{D_T}{r^2} \frac{\partial}{\partial r}\left(r^2 \frac{\partial P_T}{\partial r}\right) = 0, \qquad (10)$$

where P_T and D_T are the partial pressure and diffusivity, respectively, in the tissue.

In the blood compartment, the rate of change of capillary blood partial pressure, $P_C(t)$, must be balanced with the net gas delivery through perfusion and the diffusive flux through the tissue–blood interface:

$$V_C \frac{d}{dt}(\beta_C P_C) = \dot{Q}(\beta_{\bar{V}} P_{\bar{V}} - \beta_C P_C) - 4\pi[R_S(t)$$

$$+h]^2 D_T \beta_T \frac{\partial P_T}{\partial r}\bigg|_{r=R_S(t)+h}. \qquad (11)$$

Venous blood enters the compartment at a constant flow rate $\dot{Q}$ with a constant, mixed venous partial pressure of gas, $P_{\bar{V}}$, while capillary blood exits with a time-dependent capillary partial pressure of gas, $P_C(t)$. The first term on the right-hand side of Eq.
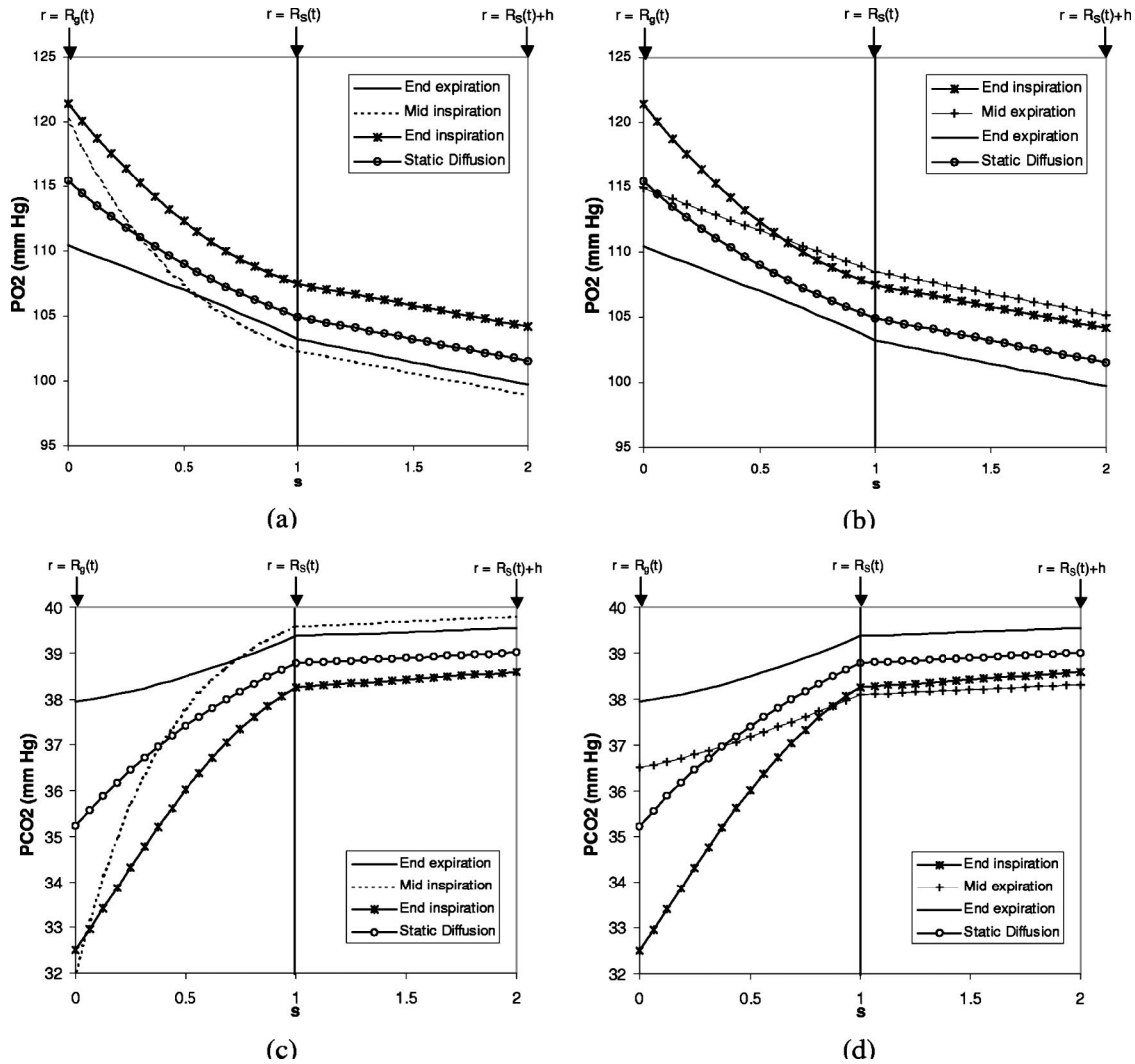
Fig. 5 Partial pressure profiles in the PFC and tissue layers during PLV: (*a*) PO_2 during inspiration, (*b*) PO_2 during expiration, (*c*) PCO_2 during inspiration, (*d*) PCO_2 during expiration. The static diffusion profile is plotted for comparison. Significant partial pressure gradients are seen in the PFC layer. Gradients are larger in the convective model during inspiration compared to static diffusion. Profiles are linear in the tissue. *s* is a normalized radial coordinate [see Eq. (21)]. The scale of the tissue layer is greatly exaggerated.

(11) represents the net gas delivery to the compartment by this process of perfusion, while the second term represents the diffusive flux of gas at the blood-respiratory membrane interface. $\beta_{\bar{V}}$ and β_C are the *effective* gas solubilities in venous and capillary blood, respectively, which are not constant, but nonlinear functions of the gas partial pressure. They are determined from blood–gas dissociation relationships as described below.

Both O_2 and CO_2 are present in different forms in blood. A small fraction of the total blood gas content of O_2 and CO_2 is found dissolved in plasma. Most of the O_2 is bound to hemoglobin while most of the CO_2 is in the form of bicarbonate ions or bound to hemoglobin and plasma proteins [25]. The total blood gas content C of these gases at any partial pressure P can be expressed as

$$C = \beta_P P + \gamma \phi(P), \tag{12}$$

where β_P is the constant solubility of the gas in plasma and $\phi(P)$ is a nonlinear function of the partial pressure. The linear term represents the portion dissolved in plasma, while the nonlinear term gives the chemically bound portion. For O_2, $\phi(P)$ is the oxyhemoglobin saturation and γ is the oxygen carrying capacity of hemoglobin. The value

$$\gamma = 20.1 \tag{13}$$

is obtained as the product of the hemoglobin content of blood [15 g/(100 ml blood)] and the binding capacity of hemoglobin [1.34 ml O_2/(g hemoglobin)]. We used a correlation due to Severinghaus [26] for the oxyhemoglobin saturation:

$$\phi(P) = \frac{P^3 + 150P}{P^3 + 150P + 23\,400}. \tag{14}$$

For CO_2, the equations of Kelman [27] were simplified using a value of 6.11 for the pK of blood and assuming a hematocrit of 42% to obtain

$$\gamma = 3.979, \tag{15}$$

$$\phi(P) = P^{0.665}.$$

In both cases the units of P are mm Hg. Here pK is related to the acid-base balance in blood and is defined as the negative logarithm of the equilibrium constant for the equilibrium between bicarbonate ions, hydrogen ions, and dissolved carbon dioxide [25].
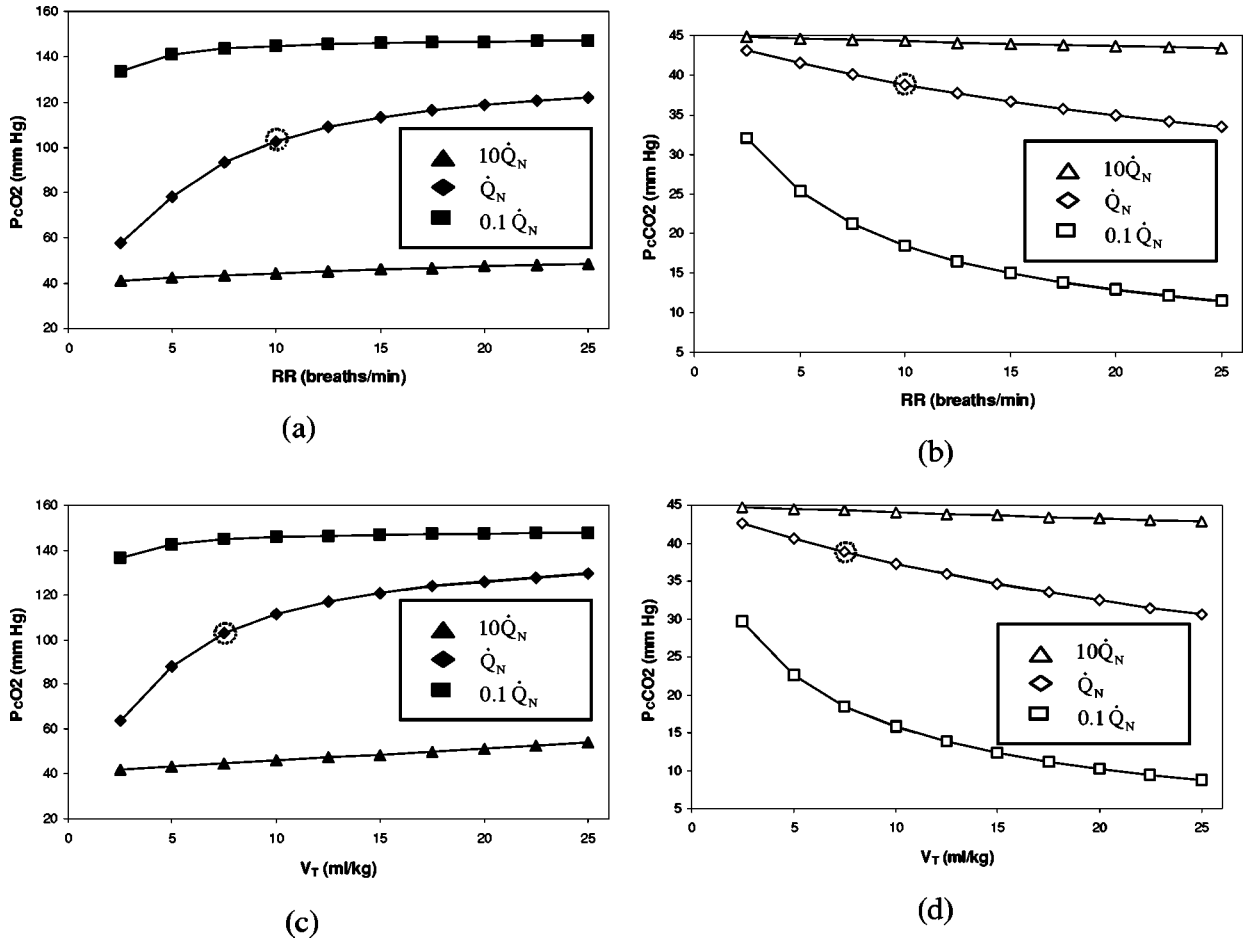
Fig. 6 Effect of varying RR at V_T=7.5 ml/kg [(a) and (b)] and varying V_T at RR=10 breaths/min [(c) and (d)] on $P_C O_2$ and $P_C CO_2$. $\dot{Q}_N$=3.57×10^{-4} ml/min; circled points correspond to $\dot{V}_A / \dot{Q} \approx 1$.

Using Eqs. (12)–(15) effective solubilities for O_2 and CO_2, β_C, and $\beta_{\bar{V}}$ in capillary and mixed venous blood, respectively, are defined as

$$\beta_c = \frac{C}{P_c(t)},$$
$$\beta_{\bar{V}} = \frac{C}{P_{\bar{V}}}. \tag{16}$$

Note, that β_C and $\beta_{\bar{V}}$ are not constant, but depend on the partial pressure. In addition, β_C is a function of time since the capillary partial pressure is time dependent.

Boundary conditions for Eqs. (7) and (10) are obtained by equating the partial pressures in adjoining compartments at the interface between them:

$$P_{PFC}(r,t) = P_g(t) \quad \text{at } r = R_g(t), \tag{17}$$

$$P_{PFC}(r,t) = P_T(r,t) \quad \text{at } r = R_S(t), \tag{18}$$

$$P_T(r,t) = P_C(t) \quad \text{at } r = R_S(t) + h. \tag{19}$$

In addition, conservation of mass at the PFC–tissue interface requires the diffusive fluxes in the two compartments to be equal.

$$D_{PFC} \beta_{PFC} \frac{\partial P_{PFC}}{\partial r} = D_T \beta_T \frac{\partial P_T}{\partial r} \quad \text{at } r = R_S(t). \tag{20}$$

The system of coupled partial and ordinary differential equations was discretized using a finite volume scheme with implicit time stepping and upwinding for the convective terms. An iterative

procedure was used to solve the resulting nonlinear equations. At the beginning of the computation the partial pressure in the sac was specified to be equal to the mixed venous value, $P_{\bar{V}}$. Computations were performed until $P_g(t)$ and $P_C(t)$ reached periodic steady states. Solutions were considered to have reached steady state when mean values of $P_g(t)$ and $P_C(t)$ over one breath did not change by more than 1% between two successive breaths. In all cases converged solutions were obtained with a grid of 80 radial points and 100 time steps per breath. A normalized radial coordinate

$$s = \begin{cases} \dfrac{r - R_g(t)}{R_S(t) - R_g(t)}, & R_g(t) < r \leq R_S(t) \\ 1 + \dfrac{r - R_s(t)}{h}, & R_S(t) < r \leq R_S(t) + h, \end{cases} \tag{21}$$

was used in the calculations, such that $s=0$ at $r=R_g(t)$, $s=1$ at $r=R_S(t)$ and $s=2$ at $r=R_S(t)+h$. Mean values of the partial pressures in the capillary blood ($P_C O_2$ for oxygen, $P_C CO_2$ for carbon dioxide) and gas compartments ($P_g O_2$, $P_g CO_2$) were computed by averaging $P_C(t)$ and $P_g(t)$ over one breath after a periodic steady state had been attained. In Sec. 3, we present results for the dependence of these averaged parameters on the system parameters.

2.3 Parameter Values. Parameter values were chosen to represent the lung anatomy and breathing pattern of a normal, adult human with a body mass of 70 kg. Weibel [28] estimates the number of alveolar sacs in an adult human to be about $N_S = 14$
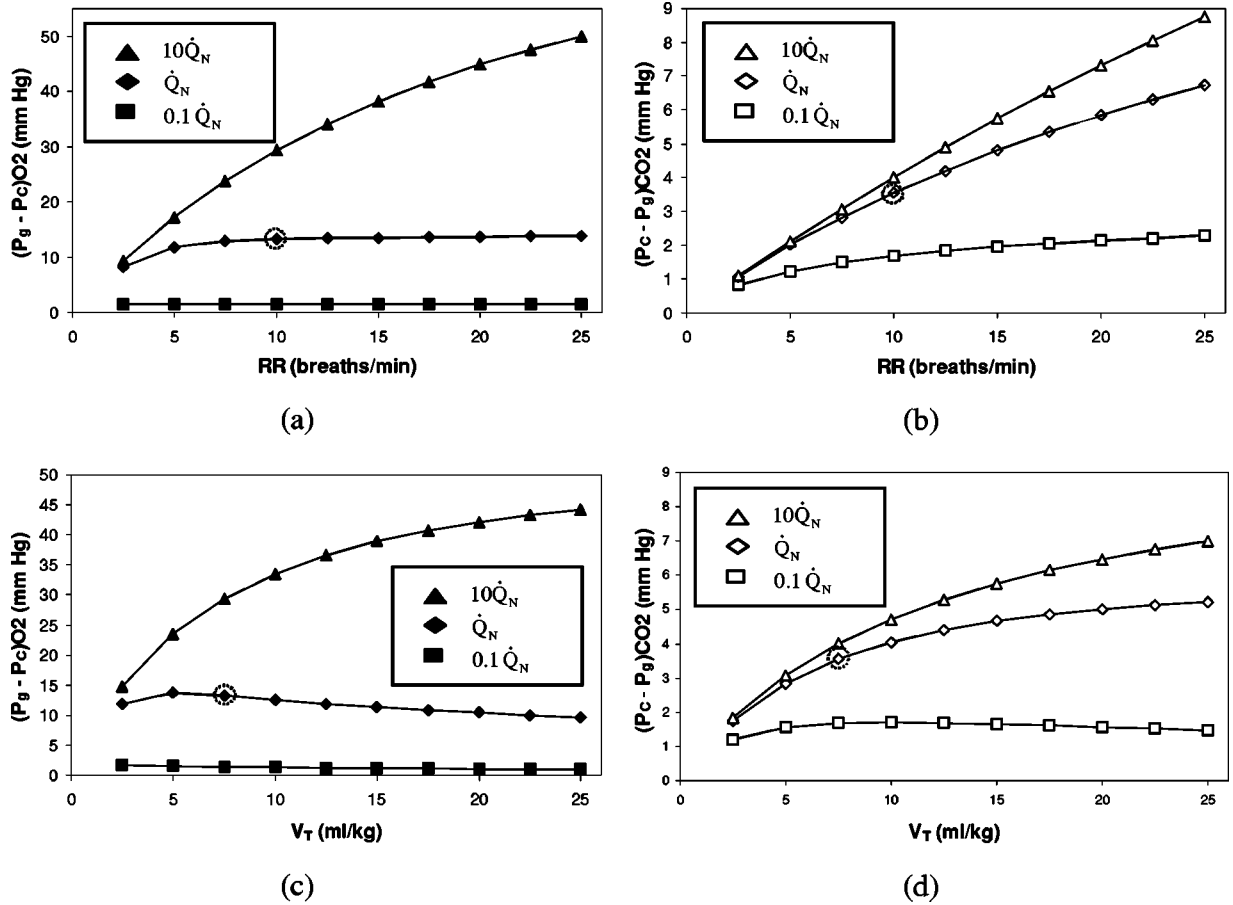
Fig. 7 Effect of varying RR at V_T=7.5 ml/kg [(a) and (b)] and varying V_T at RR=10 breaths/min [(c) and (d)] on $(P_g\text{-}P_C)O_2$ and $(P_C\text{-}P_g)CO_2$. $\dot{Q}_N$=3.57×10^{-4} ml/min. Circled points correspond to $\dot{V}_A/\dot{Q}\approx$1.

×10^6. The sac radius at functional residual capacity (FRC), R_{FRC}, is calculated by assuming the lung volume to be equally distributed among N_S spherical units, i.e., FRC=N_S ×(4π/3)R_{FRC}^3. In normal air breathing FRC=2400 ml (34.1 ml/kg) and R_{FRC}=345 μm. For PLV, a typical value of FRC=30 ml/kg has been reported in the literature [14,17]. This corresponds to a FRC of 2100 ml and R_{FRC}=330 μm. These sizes are consistent with reported measurements in human lungs [29]. Clinical trials in adult humans have used PFC doses with mean values ranging from 20 to 25 ml/kg [9,10]. We used a PFC volume of 25 ml/kg so that the sac is partially filled with liquid, resulting in a gas core radius at FRC, R_g(0)=181 μm.

In spontaneous air breathing, the normal respiratory rate is RR=15 breaths/min. The volume of fresh air inspired per breath is 500 ml, of which 350 ml ventilates the alveoli after accounting for dead space. Thus the effective tidal volume is V_T=5 ml/kg and the alveolar ventilation rate per sac is $\dot{V}_A$=(weight×V_T ×RR)/N_S=3.75×10^{-4} ml/min. In our PLV calculations we only use effective tidal volumes, V_T. In large animal experiments and human trials of conventional PLV, respiratory rates and tidal volumes in the range RR=6–20 breaths/min and V_T=8–15 ml/kg have been reported [3,6,9–11,30,31]. We examined parameter values in the range RR=2.5–25 breaths/min and V_T =2.5–25 ml/kg. In HFO+PLV respiratory rates and tidal volumes in the range RR=120–1500 breaths/min and V_T =0.25–10 ml/kg are common [19–22,32–34]. We used values in the range RR=60–900 breaths/min and V_T=0.1–5 ml/kg in our calculations. In all cases, an I:E ratio of 1:2 is used. Different combinations of V_T and RR are used to obtain alveolar ventilation

rates $\dot{V}_A$ in the range 9.38×10^{-5}–1.25×10^{-3} ml/min in conventional PLV and 1.20×10^{-4}–2.25×10^{-3} ml/min in HFO+PLV.

The normal cardiac output of an adult human is 5000 ml/min, which yields a perfusion rate $\dot{Q}_N$=3.57×10^{-4} ml/min per sac (5000 ml/14×10^6). In order to study the effect of perfusion heterogeneity in conventional PLV and HFO+PLV we considered two other perfusion rates that are 10 times larger ($\dot{Q}$=10$\dot{Q}_N$ =3.57×10^{-3} ml/min) and 10 times smaller ($\dot{Q}$=0.1$\dot{Q}_N$=3.57 ×10^{-5} ml/min) than the normal value. These choices of RR, V_T, and $\dot{Q}$ result in a wide range of $\dot{V}_A/\dot{Q}$ values. In conventional PLV, $\dot{V}_A/\dot{Q}$ varies from 2.6 to 35 at the low perfusion rate (0.1$\dot{Q}_N$), 0.26–3.5 at the normal perfusion rate ($\dot{Q}_N$) and 0.026– 0.35 at the high perfusion rate (10$\dot{Q}_N$). The corresponding ranges in HFO+PLV are 3.4–63 at the low perfusion rate, 0.34–6.3 at the normal perfusion rate, and 0.034–0.63 at the high perfusion rate. A summary of the ventilation and perfusion parameters used is provided in Table 1.

A tissue layer thickness h=0.6 μm was chosen based on the average thickness of the respiratory membrane [25]. The volume of the capillary blood compartment, V_C, was calculated by assuming the capillary network encapsulating the sac to cover 75% of the surface area with a thickness equal to the diameter of a single red blood cell, t_{RBC}=8 μm.[17] Thus, V_C=0.75 ×4$\pi R_{FRC}^2 t_{RBC}$=4.68×10^{-6} ml.

The solubilities β_P of O_2 and CO_2 in plasma are equal to 0.003 ml O_2/(100 ml blood mm Hg) and 0.057 ml CO_2/(100 ml blood mm Hg), respectively. Lango et al. [35] have tabulated solu-
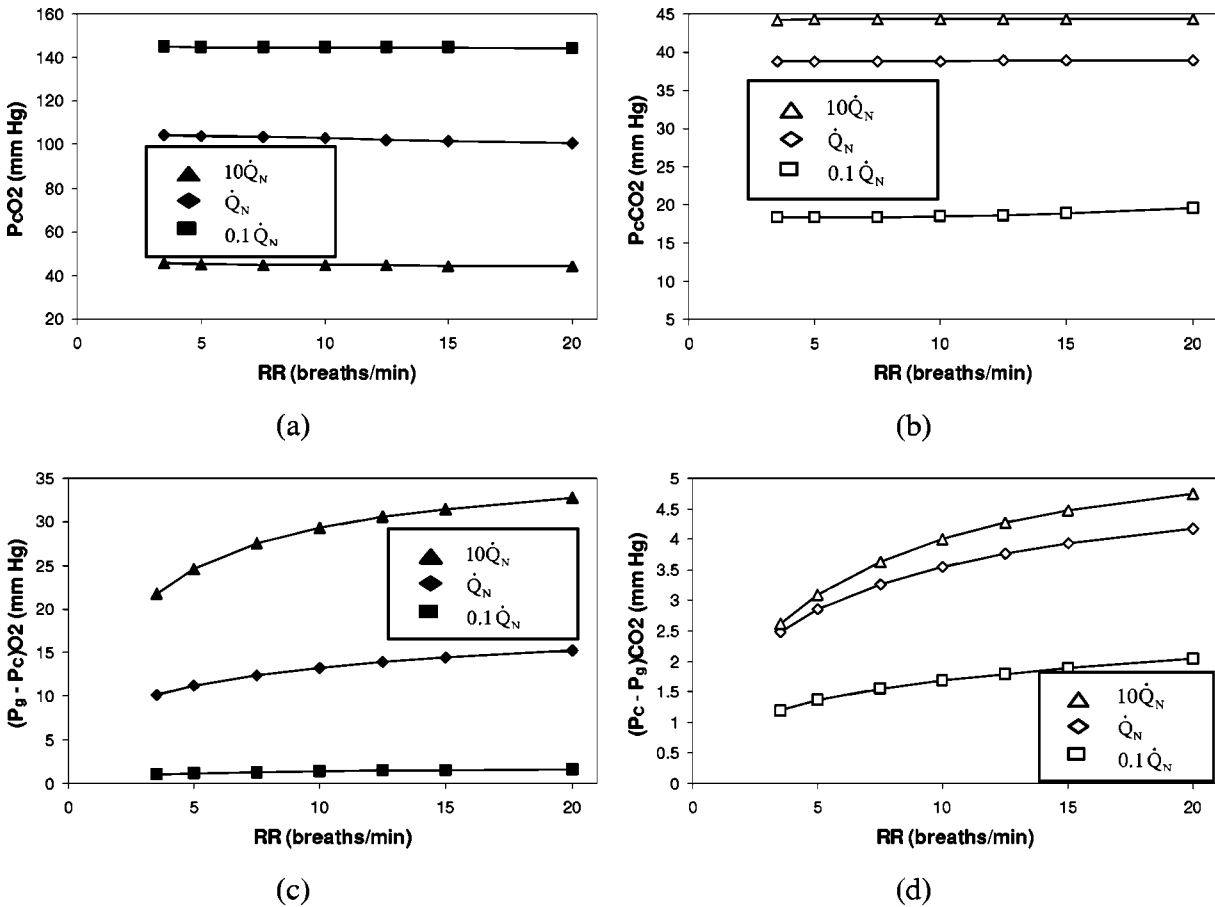
Fig. 8 Effect of varying RR and V_T at constant $\dot{V}_A$ on (a) $P_C O_2$, (b) $P_C CO_2$, (c) $(P_g\text{-}P_C)O_2$, (d) $(P_C\text{-}P_g)CO_2$. $\dot{Q}_N = 3.57 \times 10^{-4}$ ml/min.

bilities of various gases in biological media. Their data indicate that the solubility of O_2 in the tissue layer β_T is equal to the solubility in plasma. Since no data were available for CO_2 we assumed that the solubility of CO_2 in lung tissue is also equal to its solubility in plasma. Solubilities of O_2 and CO_2 in PFC were taken from VanLöbensels et al. [17] who measured solubilities in the PFC Perflubron. Tham et al. [36] measured diffusion coefficients of O_2 and CO_2 in three PFCs (Caroxin-D, Caroxin-F, and FC-80) and found mean values of $D_{PFC} = 5.61 \times 10^{-5}$ cm²/s for O_2 and $D_{PFC} = 4.36 \times 10^{-5}$ cm²/s for CO_2. In comparison the corresponding diffusivities in air at 37°C are 0.190 cm²/s (O_2) and 0.147 cm²/s (CO_2). Lango et al. [35] estimate that the gas diffusivities in tissue vary from 25% to 50% of the diffusivity in water at the same temperature. We used values for the tissue diffusivity $D_T = 1.2 \times 10^{-5}$ cm²/s for O_2 and $D_T = 0.96 \times 10^{-5}$ cm²/s for CO_2 which correspond to 40% of the values in water at 37°C. Solubility and diffusivity values are summarized in Table 2.

3 Results

3.1 Partial Pressure Profiles. In order to validate the model we simulated normal air breathing with the parameter val-

Table 3 Combinations of RR and V_T used to obtain $\dot{V}_A = 3.75 \times 10^{-4}$ ml/min

RR (breaths/min)	3.5	5	7.5	10	12.5	15	20
V_T (ml/kg)	21.43	15	10	7.5	6	5	3.75

ues listed in Table 1. In air breathing the annular region between the gas core and the tissue layer is gas filled. The governing equations were solved using the physical properties of air instead of PFC. Mean values of the capillary partial pressures over one breath ($P_C O_2$ and $P_C CO_2$) were computed when the solutions attained a periodic state. $P_C O_2$ reached a steady state value of 108 mm Hg in 17 breaths while $P_C CO_2$ reached a steady state value of 38.5 mm Hg in ten breaths.

Figure 4 shows PO_2 and PCO_2 profiles in the gas-filled annular region and the tissue layer at different times during the breathing cycle. For comparison, a static diffusion profile is also plotted. This static profile was obtained as follows: First, the mean radii of the sac and gas core over one breath were computed for the parameters in Table 1. Then the steady diffusion equation [Eq. (7) without the convective and time derivative terms] was solved in this model using a flow-through gas compartment as described in [14]. This nonconvective model cannot describe second-to-second changes in tidal breathing and thus the static diffusion result represents an average profile when convective effects due to the oscillatory motion of the sac are neglected.

As expected, both PO_2 and PCO_2 are almost constant in the sac because of the relatively large diffusivities of O_2 and CO_2 in air and linear in the tissue layer. In the convective model Péclet number is small, about 0.01. PO_2 is seen to be maximum at end inspiration and minimum at end expiration. The opposite is true for PCO_2. These results confirm that the mathematical model and numerical scheme result in time periodic solutions and reproduce mean partial pressures and profiles that are in agreement with well-established results for air breathing. Convection has very
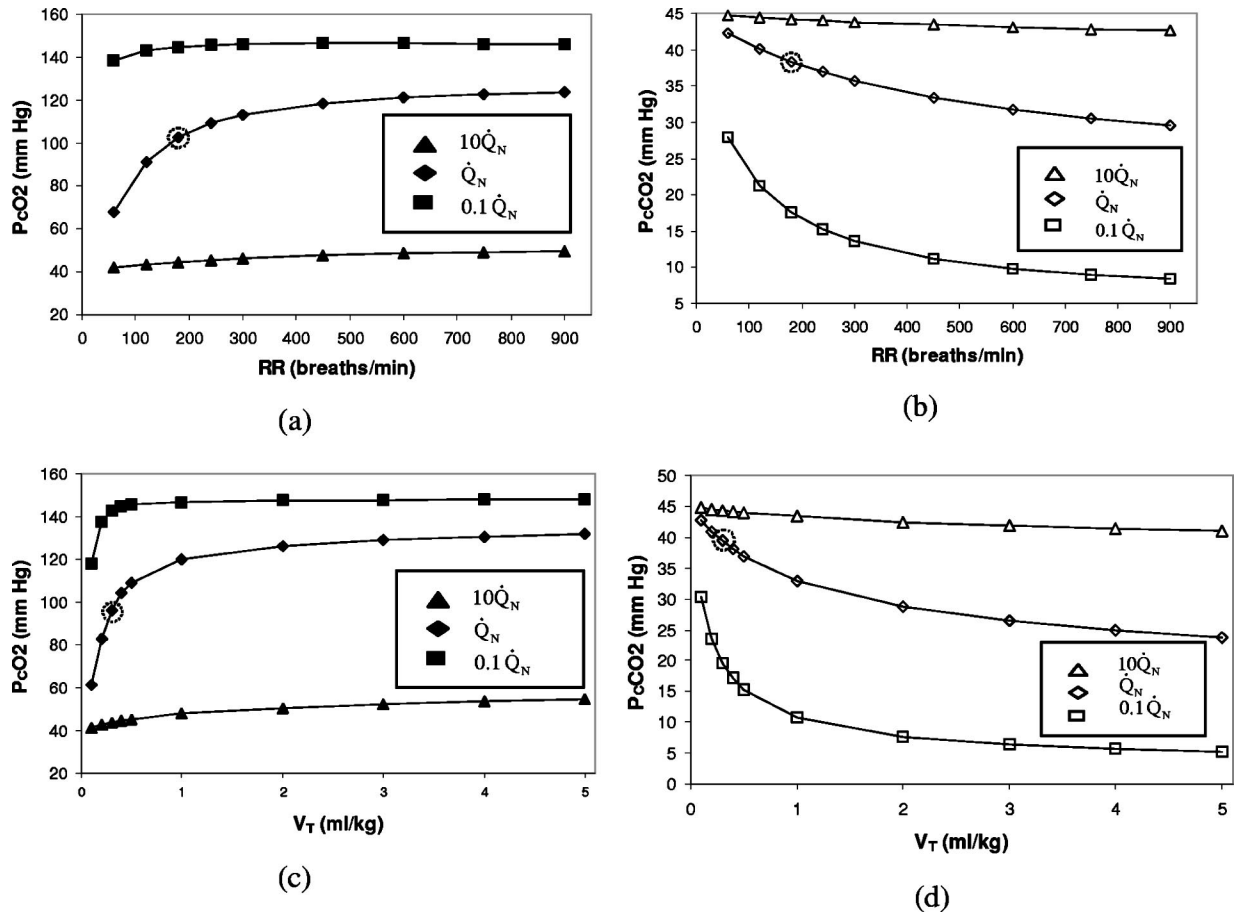
Fig. 9 Effect of varying RR at $V_T = 0.5$ ml/kg [(*a*) and (*b*)] and V_T at RR=240 breaths/min [(*c*) and (*d*)] on $P_C O_2$ and $P_C CO_2$. $\dot{Q}_N = 3.57 \times 10^{-4}$ ml/min; circled points correspond to $\dot{V}_A / \dot{Q} \approx 1$; $\dot{Q}_N = 3.57 \times 10^{-4}$ ml/min; circled points correspond to $\dot{V}_A / \dot{Q} \approx 1$.

little effect because Pe is very small. As a result, the static diffusion profile is qualitatively similar to the profiles from the convective model.

PO_2 and PCO_2 profiles during PLV are shown in Fig. 5 for RR=10 breaths/min, $V_T = 7.5$ ml/kg and $\dot{Q} = \dot{Q}_N = 3.57 \times 10^{-4}$ ml/min. This choice of parameters matches $\dot{V}_A$ and $\dot{Q}$ values used for the air breathing calculations and allows a direct comparison between GV and PLV. The corresponding static diffusion profile is also plotted. In each case significant partial pressure gradients exist within the PFC layer and the profiles are curved, most noticeably during inspiration. The static diffusion profile also shows partial pressure gradients due to the relatively low diffusivities of O_2 and CO_2 in PFC. These gradients are smaller than the gradients in the convective model during inspiration, but larger during expiration. The difference in partial pressures between the gas side ($s=0$) and the capillary side ($s=2$) ranges from 9 to 22 mm Hg for O_2 and from 1 to 8 mm Hg for CO_2 in the convective model. The corresponding differences in static diffusion are 14 mm Hg (O_2) and 4 mm Hg (CO_2). These differences are a measure of the driving force for gas transfer and are greatest at midinspiration and smallest at midexpiration in the convective model. This suggests that gas exchange rates at the alveolar-blood boundary are highest in the period between mid- and end-inspiration when both partial pressure gradients and surface area are large.

3.2 Effect of Varying $\dot{V}_A$. Variations in regional ventilation and redistribution of blood flow in a PFC filled lung results in local values of $\dot{V}_A$, $\dot{Q}$, and $\dot{V}_A/\dot{Q}$ varying widely in different regions of the lung. In order to study the effect of regional inhomogeneities in these quantities on gas exchange, we performed calculations over a wide range of $\dot{V}_A$ for low, normal, and high values of $\dot{Q}$. Since $\dot{V}_A$ can be varied by changing either RR or V_T we considered two cases: (1) V_T fixed at 7.5 ml/kg, RR varies from 2.5 to 25 breaths/min and (2) RR fixed at 10 breaths/min, V_T varies from 2.5 to 25 ml/kg. These choices for RR and V_T result in $\dot{V}_A$ varying from 9.38×10^{-5} to 1.25×10^{-3} ml/min while $\dot{V}_A/\dot{Q}$ values range from 2.6 to 35 at $0.1\dot{Q}_N$, 0.26 to 3.5 at $\dot{Q}_N$, and 0.026 to 0.35 at $10\dot{Q}_N$.

Figures 6–8 show the effect of varying RR or V_T on average partial pressures in the gas and blood for different values of $\dot{Q}$. Figure 6 shows that the average partial pressure of oxygen in blood, $P_C O_2$, increases while that of carbon dioxide, $P_C CO_2$, decreases with increasing RR or V_T. In each graph the point corresponding to matched ventilation perfusion ($\dot{V}_A/\dot{Q} \approx 1$) is marked with a circle. At these points the capillary partial pressures ($P_C O_2 = 102.8$ mm Hg, $P_C CO_2 = 38.8$ mm Hg) are close to their normal values. The deviation of $P_C O_2$ and $P_C CO_2$ from their normal values depends on the degree of mismatch between ventilation and perfusion. Figure 6 indicates that $P_C O_2$ is most sensitive to changes in RR or V_T when $\dot{Q} = \dot{Q}_N$ and $\dot{V}_A/\dot{Q}$ varies from 0.26 to 3.5. When the mismatch between ventilation and perfusion is much greater ($\dot{V}_A/\dot{Q} \gg 1$ for $0.1\dot{Q}_N$ or $\dot{V}_A/\dot{Q} \ll 1$ for $10\dot{Q}_N$), $P_C O_2$ is quite insensitive to changes in RR or V_T. In contrast $P_C CO_2$ changes significantly at $0.1\dot{Q}_N$ and normal $\dot{Q}_N$.

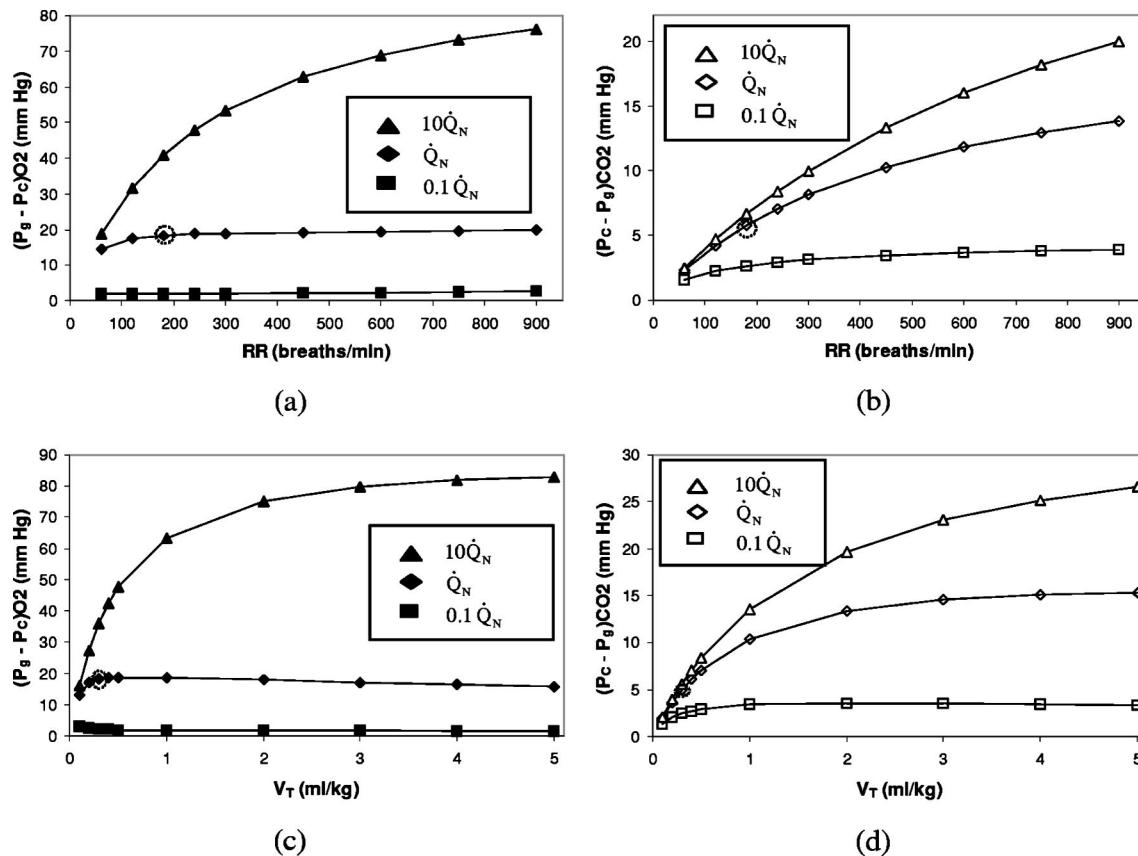Figure 7 shows the effect of varying RR and V_T on $(P_g - P_C)O_2$

Fig. 10 Effect of varying RR at $V_T=0.5$ ml/kg [(a) and (b)] and V_T at RR=240 breaths/min [(c) and (d)] on $(P_g\text{-}P_C)O_2$ and $(P_C\text{-}P_g)CO_2$. $\dot{Q}_N=3.57\times10^{-4}$ ml/min; circled points correspond to $\dot{V}_A/\dot{Q}\approx1$.

and $(P_C\text{-}P_g)CO_2$ which are measures of alveolar-arterial pressure differences $[(A\text{-}a)DO_2$ and $(a\text{-}A)DCO_2]$. In contrast to GV, non-zero pressure differences are found even at matched ventilation–perfusion ratios $[(P_g\text{-}P_C)O_2=10.6$ mm Hg, $(P_C\text{-}P_g)CO_2=3.5$ mm Hg]. Figures 7(a)–7(b) show that both $(P_g\text{-}P_C)O_2$ and $(P_C\text{-}P_g)CO_2$ increase with increasing RR. The differences are small at low perfusion rates, $0.1\dot{Q}_N$ and do not change much with RR or V_T. $(P_g\text{-}P_C)O_2$ magnitudes and variations with RR are significantly larger at high perfusion rates, $10\dot{Q}_N$ compared to normal perfusion rates, $\dot{Q}_N$. In contrast $(P_C\text{-}P_g)CO_2$ values are comparable at $\dot{Q}_N$ and $10\dot{Q}_N$ (<2 mm Hg difference). When V_T is varied at constant RR different behavior is seen in Figs. 7(c)–7(d): $(P_g\text{-}P_C)O_2$ passes through a maximum with increasing V_T at $\dot{Q}_N$ while $(P_C\text{-}P_g)CO_2$ passes through a maximum at $0.1\dot{Q}_N$. The fact that these maxima are not seen for similar $\dot{V}_A$ and $\dot{Q}$ values in Figs. 7(a)–7(b) indicates that $(P_g\text{-}P_C)O_2$ and $(P_C\text{-}P_g)CO_2$ are affected by the particular combination of RR and V_T used to obtain a given $\dot{V}_A$.

3.3 Effect of Varying RR or V_T at Constant $\dot{V}_A$. A given ventilation rate $\dot{V}_A$ can be obtained using different combinations of RR and V_T. A high RR-low V_T combination results in a shorter breathing period and smaller surface area compared to a low RR-high V_T combination. We studied how these changes in the alveolar dynamics affect gas exchange by using different V_T-RR combinations listed in Table 3 to provide a constant value of $\dot{V}_A=3.75\times10^{-4}$ ml/min. This particular value of $\dot{V}_A$ was chosen to provide $\dot{V}_A/\dot{Q}\approx1$ ratios when $\dot{Q}=\dot{Q}_N$. Capillary partial pressures and $P_C\text{-}P_g$ differences are plotted in Fig. 8 for different

values of $\dot{Q}$. In these figures RR increases as one moves from left to right and the corresponding V_T decreases to maintain $\dot{V}_A$ constant. In Figs. 8(a)–8(b) $P_C O_2$ decreases slightly (less than 4 mm Hg) and $P_C CO_2$ increases slightly (less than 2 mm Hg) with increasing RR. Variations are quite small, but $P_C O_2$ changes more than $P_C CO_2$. As in Figs. 7(a)–7(b), $P_C O_2$ is most sensitive at $\dot{Q}=\dot{Q}_N$ while $P_C CO_2$ is most sensitive at $\dot{Q}=0.1\dot{Q}_N$. Thus a high RR-low V_T combination results in a very slight deterioration in gas exchange, quantified by lower $P_C O_2$ and higher $P_C CO_2$ values. To explain this observation, note that increasing RR results in a faster flow while increasing V_T leads to a larger surface area as well as faster flow. The combination of these two effects results in less efficient gas exchange at a high RR-low V_T combination compared to a low RR-high V_T one at any given $\dot{V}_A$. Figures 8(c)–8(d) indicate that $P_C\text{-}P_g$ differences are more sensitive to RR-V_T combinations for both O_2 and CO_2. For both gases $P_C\text{-}P_g$ values increase by 50%–66% as RR is increased. Variations with RR are most significant at $10\dot{Q}_N$ for O_2 while they are of similar magnitude at $\dot{Q}_N$ and $10\dot{Q}_N$ for CO_2.

3.4 High Frequency Oscillation With PLV (HFO+PLV). The previous results indicate that increasing RR and decreasing V_T while maintaining a given ventilation rate results in lower $P_C O_2$, higher $P_C CO_2$ and larger $P_C\text{-}P_g$ differences. These trends become more pronounced in HFO+PLV where very high respiratory rates are used in conjunction with small tidal volumes. We studied gas exchange with parameter values relevant to the high frequency regime in order to determine how gas exchange is affected under these conditions.

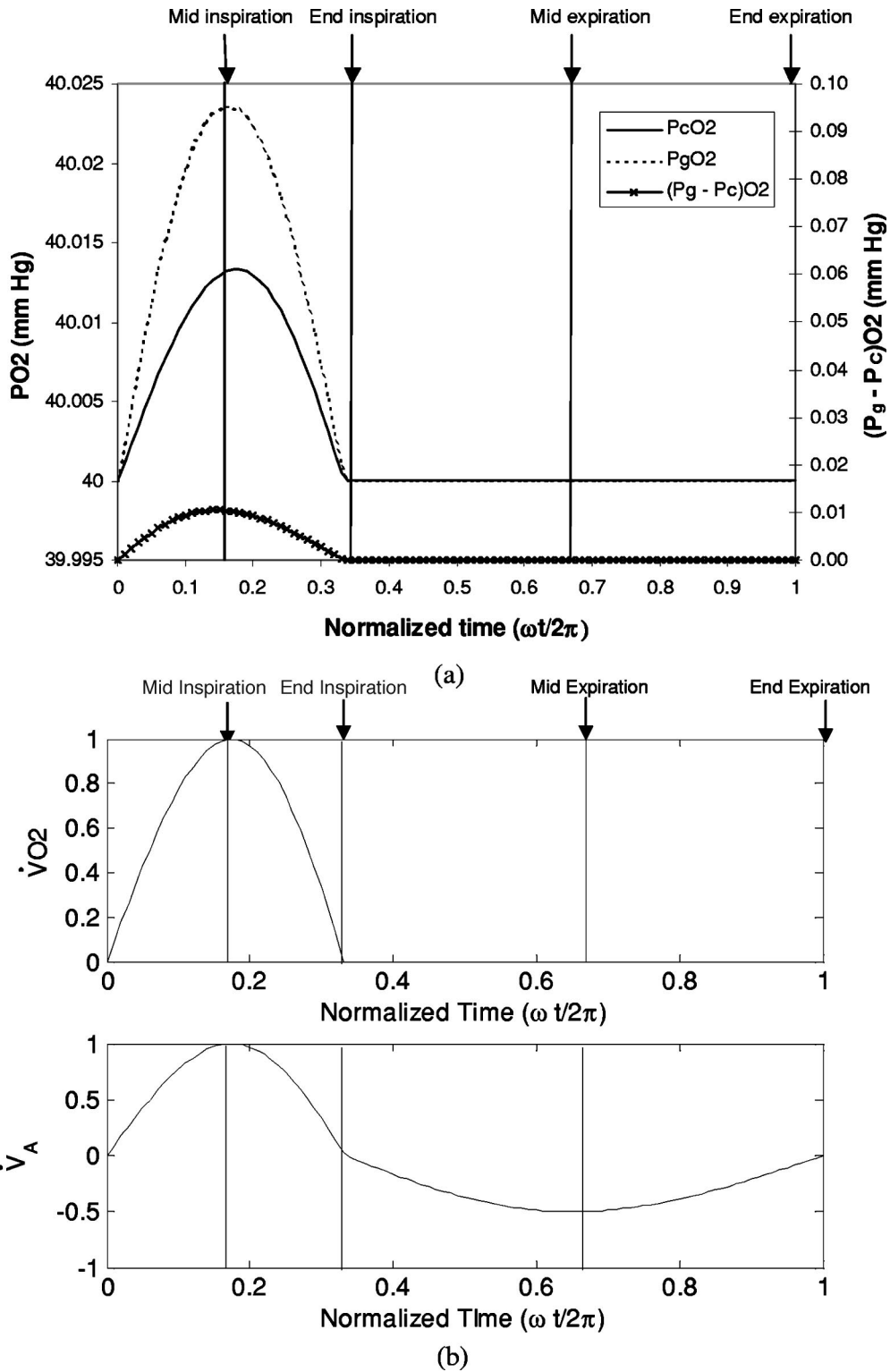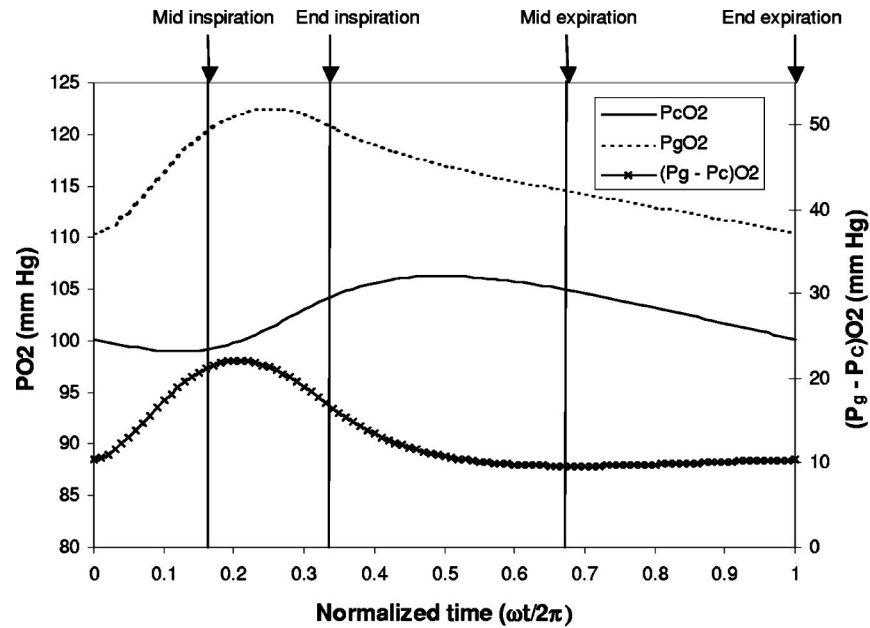As in the case of conventional PLV, $\dot{V}_A$ was varied first at

Fig. 11 Variation of (a) $P_C O_2$, $P_g O_2$ (left axis), $(P_g - P_C)O_2$ (right axis) and (b) dimensionless ventilation ($\dot{V}_A$) and mass transfer ($\dot{V}O_2$) rates over one breath for $P_e = 0.001$. $\dot{V}_A$ and $\dot{V}O_2$ are scaled with their peak values.

constant V_T and then at constant RR at $\dot{Q} = 0.1\dot{Q}_N$, $\dot{Q}_N$, and $10\dot{Q}_N$. In the first case, RR was varied in the range 60–900 breaths/min at $V_T = 0.5$ ml/kg. In the second case, RR was fixed at 240 breaths/min and V_T varied from 0.1 to 5 ml/kg. These ranges of RR and V_T result in $\dot{V}_A$ values in the range $1.20 \times 10^{-4} – 2.25$

$\times 10^{-3}$ ml/min. $\dot{V}_A / \dot{Q}$ values lie in the range 3.4–63 at $0.1\dot{Q}_N$, 0.34–6.3 at $\dot{Q}_N$, and 0.034–0.63 at $10\dot{Q}_N$. These values are higher than the ones in the conventional PLV calculations.

Capillary partial pressures and P_C-P_g differences are plotted in Figs. 9 and 10. As seen in Figs. 9(a) and 9(b), $P_C O_2$ increases and
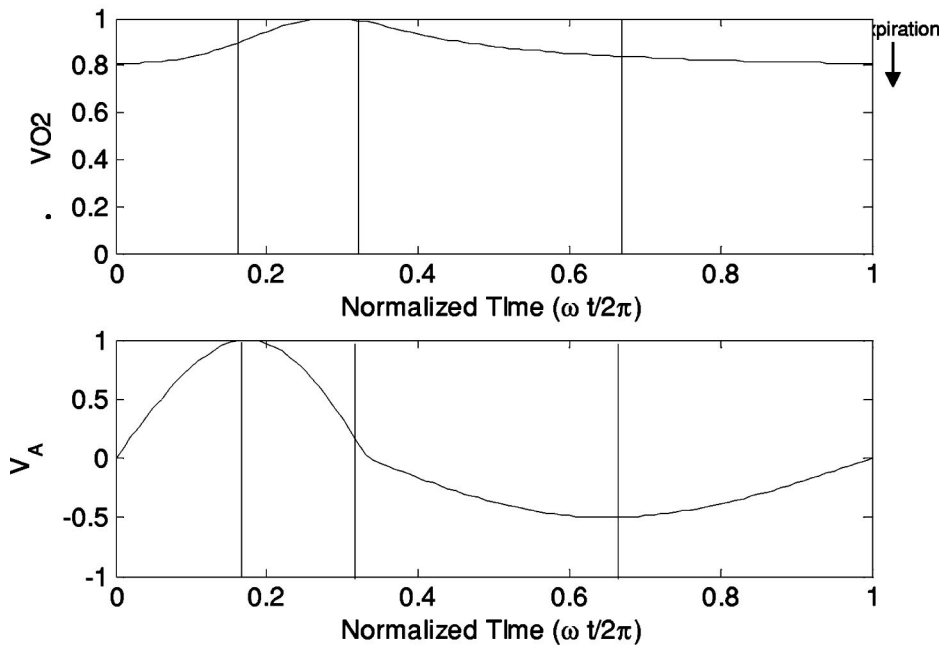
Fig. 12 Variation of (*a*) $P_C O_2$, $P_g O_2$ (left axis), (P_g-P_C)O_2 (right axis) and (*b*) dimensionless ventilation ($\dot{V}_A$) and mass transfer ($\dot{V}O_2$) rates over one breath for P_e=20. $\dot{V}_A$ and $\dot{V}O_2$ are scaled with their peak values.

$P_C CO_2$ decreases with increasing RR or V_T. At matched ventilation-perfusion $(\dot{V}_A/\dot{Q} \approx 1)$ $P_C O_2$=96.2 mm Hg and $P_C CO_2$=39.4 mm Hg. While $P_C CO_2$ is almost equal to its value in conventional PLV, $P_C O_2$ is 5–9 mm Hg lower. These results are consistent with Fig. 8, which showed that at a given $\dot{V}_A$ gas exchange is less efficient at high RR-low V_T combinations and that O_2 exchange is affected more than CO_2 exchange. However decrease in gas exchange is sufficiently small so that it is possible to maintain normal blood gas levels. P_C-P_g differences are plotted in Fig. 10. (P_g-P_C)O_2 values are comparable to conventional PLV at $0.1\dot{Q}_N$ and $\dot{Q}_N$, but are much larger at $10\dot{Q}_N$. At this high

perfusion rate (P_g-P_C)O_2 values are comparable to or even exceed $P_C O_2$. (P_C-P_g)CO_2 values are much higher than in conventional PLV at $\dot{Q}_N$ and $10\dot{Q}_N$ and are as high as 55% of the $P_C CO_2$ values. Thus very large P_C-P_g differences occur in high frequency PLV.

4 Discussion

The convective model described here differs significantly from the nonconvective model of VanLöbensels et al. [17], which modeled static diffusion across a stagnant layer of PFC with no tidal ventilation. They accounted for changes in lung volume by com-

puting steady state P_C and P_g values at different sac radii corresponding to end expiratory and end inspiratory conditions. This is a quasistatic, Pe≪1, approach which assumes that the capillary and gas side pressure quickly equilibrate to their steady state values after a volume change. As the authors point out, this may more accurately represent the effect of breath holding rather than tidal ventilation. Using this approach they found that P_C-P_g differences are smallest at end inspiration when the PFC layer is thinnest and largest at end expiration when the PFC layer is thickest, as one would expect in static diffusion. We show that very different results are obtained when tidal ventilation is included in a PLV model. The typical time required to reach steady state in a system with length scale R and diffusivity D is $T_D \sim R^2/D$. In PLV, $T_D \sim 18$ s for a sac of radius $R = 300 \mu$m and $D = 5 \times 10^{-5}$ cm^2/s. The typical time scale of ventilation over which lung volume changes is $T_V \sim 1/\omega = 1/(2\pi RR/60) = 1$ s for a breathing rate RR=10 breaths/min. The ratio $T_D/T_V \sim \omega R^2/D$ is the Péclet number, Pe, whose magnitude is 0.001–0.01 in GV and 15–50 in PLV. Low values of Pe in GV indicate that diffusion is fast compared to ventilation and the quasistatic assumption is valid. However, in PLV there is insufficient time for the equilibration of gas and capillary side partial pressures and therefore it is not appropriate to model the effects of ventilation by steady state solutions at different lung volumes.

In order to quantify the effect of nonzero Pe on P_C and P_g in PLV, we compared two cases, one with a very low respiratory rate RR=5×10^{-4} breaths/minute (Pe=0.001) and a second with a normal respiratory rate RR=10 breaths/minute (Pe=20). In each case the other parameters were fixed at FRC=30 ml/kg, V_T =7.5 ml/kg, PFC dose=25 ml/kg, and $\dot{Q} = \dot{Q}_N = 3.57 \times 10^{-4}$ ml/min. For the low Pe, $P_C O_2$, $P_g O_2$, and $(P_g$-$P_C)O_2$ are plotted over one breath in Fig. 11(a). Dimensionless forms of the sac radius, $R_S(t)$, the ventilation rate $\dot{V}_A$ $= 4\pi R_S^2(t) dR_S(t)/dt$ and the mass transfer rate $\dot{V}O_2$ are shown in Fig. 11(b). $R_S(t)$ is scaled with R_{FRC} while $\dot{V}_A$ and $\dot{V}O_2$ are scaled with their maximum values over one breath. Figures 12(a) and 12(b) show the same quantities for the higher Pe. When Pe =0.001, $P_C O_2$, $P_g O_2$, $(P_g$-$P_C)O_2$, $\dot{V}_A$ and $\dot{V}O_2$ are all in phase. During the inspiratory phase of the cycle pressures and mass transfer rate increase with $\dot{V}_A$ and reach their maximum values at mid inspiration, when $\dot{V}_A$ is highest. $P_C O_2$ and $P_g O_2$ decrease during the latter half of inspiration, become essentially equal by end inspiration, when $\dot{V}_A$ is zero, and remain so during the expiratory phase. Almost all the gas exchange occurs during inspiration. Thus when diffusion is fast compared to ventilation (Pe≪1) the dynamics are essentially quasistatic, i.e., the capillary side reacts almost instantaneously to changes in the gas side pressures.

The situation is quite different for larger Pe, as seen in Fig. 12. When Pe≫1, $P_C O_2$ requires a finite time to respond to changes in $P_g O_2$ resulting from ventilation. Therefore the partial pressures are no longer in phase and $P_C O_2$ lags behind $P_g O_2$ as seen in Fig. 12(a). This phase difference leads to some counterintuitive results. For instance, during the initial stages of inspiration, as $\dot{V}_A$ *increases*, $P_C O_2$ *decreases*. However $P_g O_2$ increases and the net effect leads to higher P_C-P_g differences when ventilation is increased holding perfusion constant. At end inspiration, $P_C O_2$ is increasing while $P_g O_2$ is decreasing. As a result $(P_g$-$P_C)O_2$ is not minimum when the PFC layer is thinnest, but at a later time in the cycle. Figure 12(b) indicates that $\dot{V}O_2$ remains higher than 80% of its peak value during expiration and the mass transfer rate remains nearly constant throughout the cycle.

4.1 Summary.
Gas transport mechanisms in GV and PLV are very different, since Péclet numbers are small in GV (Pe =0.001–0.01) compared to PLV (Pe=15–50). Significant partial pressure gradients in the PFC layer and nonzero P_C-P_g differences exist in PLV. The higher Péclet numbers in PLV result in

phase differences between P_C and P_g over the course of a breath, which contribute to the nonzero P_C-P_g values that persist throughout the respiratory cycle. The mass transfer rate is nearly constant throughout the breath when Pe≫1, but when Pe≪1 almost all the transport occurs during inspiration.

One of the aims of our modeling effort was to determine the effect of different ratios of ventilation and perfusion on gas exchange in PLV. We examined gas exchange over a wide range of ventilation rates by varying either the respiratory rate or tidal volume at low, normal, and high perfusion rates. $P_C O_2$ was found to be most sensitive to changes in ventilation at normal perfusion rates, but did not change much at low and high perfusion rates. While $P_C O_2$ was most sensitive at low perfusion rates it also showed significant changes at normal perfusion rates. $(P_g$-$P_C)O_2$ varied over a wide range at high perfusion rates and could be as large as $P_C O_2$ in conventional PLV and up to $3 \times P_C O_2$ in HFO +PLV. However, it did not vary much with the ventilation rate at low and normal perfusion rates. In contrast, $(P_C$-$P_g)CO_2$ values were comparable at normal and high perfusion rates in both conventional PLV and HFO+PLV and could be as large as 50%–66% of the $P_C CO_2$ values. A practical consequence of these large P_C-P_g differences is that expired gas partial pressures may not be accurate indicators of arterial blood gas pressures.

An interesting finding was that gas exchange depends on the particular combination of respiratory rate and tidal volume used to obtain a given ventilation rate. It was found that using a low RR-high V_T combination to achieve a given ventilation rate leads to slightly more efficient gas exchange compared to a high RR-low V_T combination as quantified by lower $P_C O_2$ and higher $P_C CO_2$. This may be one factor that can help explain clinical observations that gas exchange is not improved in HFO+PLV compared to conventional PLV [19,21,22]. The effect of different RR-V_T combinations is most noticeable in the P_C-P_g differences: Both $(P_g$-$P_C)O_2$ and $(P_C$-$P_g)CO_2$ are up to 50%–65% higher for a high RR-low V_T combination compared to a low RR-high V_T combination at the same ventilation rate.

While our work provides significant insight into the physical mechanisms responsible for transport in a PFC filled lung, the results cannot be directly compared to experimental data since the model describes transport in a single alveolar sac. Experimentally measured quantities such as arterial blood gas pressures are the weighted mean of the contributions of a number of such sacs with a heterogeneous distribution of ventilation, perfusion, and PFC volume. The partial pressure of gas entering the sac (P_{in}) is specified as an input parameter in the current model. In reality, only the partial pressure at the mouth is known and P_{in} must be calculated by accounting for diffusion and mixing in the conducting airways. A possible extension to the model would account for these transport processes in the conducting airways by incorporating the trumpet-shaped model of Paiva [37]. Finally, the sac geometry was idealized to be spherical with gas entering through the center, resulting in a radial flow field in the PFC layer. In a more accurate representation, the sac is connected to an airway through an alveolar duct that serves as a conduit for flow. Such a geometry would lead to more complicated flow patterns inside the sac [38,39] and affect convective transport. In addition, the internal geometry of the sac is not smooth, but lined with the septal walls of individual alveoli. This may lead to the formation of recirculation regions within the sac. In steady flows such regions trap liquid and lead to poor transport. However, the recirculations may exhibit temporal growth and decay during tidal ventilation and improve transport by enhancing mixing. These considerations remain to be explored in future work.

References

[1] Clark, L. C., and Gollan, F., 1966, "Survival of Mammals Breathing Organic Liquids Equilibrated With Oxygen at Atmospheric Pressure," Science, **152**, p. 1755.

[2] Curtis, S., Peek, J., and Kelly, D., 1993, "Partial Liquid Breathing With Perflubron Improves Arterial Oxygenation in Acute Canine Lung Injury," J. Appl. Physiol., **75**, pp. 2696–2702.

[3] Hirschl, R. B. et al., 1995, "Improvement of Gas Exchange, Pulmonary Function, and Lung Injury With Partial Liquid Ventilation. A Study Model in a Setting of Severe Respiratory Failure," Chest, **108**, pp. 500–508.

[4] Leach, C. L. et al., 1993, "Perfluorocarbon-Associated Gas Exchange (Partial Liquid Ventilation) in Respiratory Distress Syndrome: A Prospective, Randomized, Controlled Study," Crit. Care Med., **21**, pp. 1270–1278.

[5] Papo, M. C. et al., 1996, "Perfluorocarbon-Associated Gas Exchange Improves Oxygenation, Lung Mechanics, and Survival in a Model of Adult Respiratory Distress Syndrome," Crit. Care Med., **24**, pp. 466–474.

[6] Quintel, M. et al., 1998, "Computer Tomographic Assessment of Perfluorocarbon and Gas Distribution During Partial Liquid Ventilation for Acute Respiratory Failure," Crit. Care Med., **158**, pp. 249–255.

[7] Gauger, P. G. et al., 1996, "Initial Experience With Partial Liquid Ventilation in Pediatric Patients With the Acute Respiratory Distress Syndrome," Crit. Care Med., **24**, pp. 16–22.

[8] Greenspan, J. S. et al., 1999, "Partial Liquid Ventilation in Critically Ill Infants Receiving Extracorporeal Life Support," Pediatrics, **99**, p. E2.

[9] Hirschl, R. B. et al., 1996, "Initial Experience With Partial Liquid Ventilation in Adult Patients With the Acute Respiratory Distress Syndrome," JAMA, J. Am. Med. Assoc., **275**, pp. 383–389.

[10] Hirschl, R. B. et al., 2002, "Prospective, Randomized, Controlled Pilot Study of Partial Liquid Ventilation in Adult Acute Respiratory Distress Syndrome," Am. J. Respir. Crit. Care Med., **165**, pp. 781–787.

[11] Leach, C. L. et al., 1996, "Partial Liquid Ventilation With Perflubron in Premature Infants With Severe Respiratory Distress Syndrome: The LiquiVent Study Group," N. Engl. J. Med., **335**, pp. 761–767.

[12] Doctor, A. et al., 1998, "Pulmonary Blood Flow Distribution During Partial Liquid Ventilation," J. Appl. Physiol., **84**, pp. 1540–1550.

[13] Morris, K. P. et al., 2002, "Distribution of Pulmonary Blood Flow in the Perfluorocarbon-Filled Lung," Intensive Care Med., **26**, pp. 756–763.

[14] Mates, E. A. et al., 1997, "Shunt and Ventilation-Perfusion Distribution During Partial Liquid Ventilation in Healthy Piglets," J. Appl. Physiol., **82**, pp. 933–942.

[15] Lim, C. M. et al., 2001, "Effect of Increasing Perfluorocarbon Dose on V(Over Dot)A/Q(Over Dot) Distribution During Partial Liquid Ventilation in Acute Lung Injury," Anesthesiology, **94**, pp. 637–642.

[16] Harris, R. S. et al., 2002, "Regional VA, Q, and VA/Q During PLV: Effects of Nitroprusside and Inhaled Nitric Oxide," J. Appl. Physiol., **92**, pp. 297–312.

[17] van Lobensels, E. M., Anderson, J. C., Hildebrandt, J., and Hlastala, M. P., 1999, "Modeling Diffusion Limitation of Gas Exchange in Lungs Containing Perfluorocarbon," J. Appl. Physiol., **86**, pp. 273–284.

[18] Cox, P. N. et al., 1997, "Concealed Air Leak Associated With Large Tidal Volumes in Partial Liquid Ventilation," Am. J. Respir. Crit. Care Med., **156**, pp. 992–997.

[19] Doctor, A. et al., 2001, "High-Frequency Oscillatory Ventilation of the Perfluorocarbon-Filled Lung: Dose-Response Relationships in an Animal Model of Acute Lung Injury," Crit. Care Med., **29**, pp. 847–854.

[20] Gothberg, S. et al., 2002, "High-Frequency Oscillatory Ventilation and Partial Liquid Ventilation After Acute Lung Injury in Premature Lambs With Respiratory Distress Syndrome," Crit. Care Med., **28**, pp. 2450–2456.

[21] Smith, K. M. et al., 1997, "Partial Liquid Ventilation: a Comparison Using Conventional and High-Frequency Techniques in an Animal Model of Acute Respiratory Failure," Crit. Care Med., **25**, pp. 1179–1186.

[22] Smith, K. M. et al., 1997, "Prolonged Partial Liquid Ventilation Using Conventional and High-Frequency Ventilatory Techniques: Gas Exchange and Lung Pathology in an Animal Model of Respiratory Distress Syndrome," Crit. Care Med., **25**, pp. 1888–1897.

[23] Sukumar, M. et al., 1998, "High-Frequency Partial Liquid Ventilation in Respiratory Distress Syndrome: Hemodynamics and Gas Exchange," J. Appl. Physiol., **84**, pp. 327–334.

[24] Gefen, A., Elad, D., and Shiner, R. J., 1999, "Analysis of Stress Distribution in the Alveolar Septa of Normal and Simulated Emphysematic Lungs," J. Biomed. Opt., **32**, pp. 891–897.

[25] Guyton, A. C., 1986, *Textbook of Medical Physiology*, 7th ed., W. B. Saunders Company, Philadelphia.

[26] Severinghaus, J. W., 1979, "Simple, Accurate Equations for Human-Blood O_2 Dissociation Computations," J. Appl. Physiol.: Respir., Environ. Exercise Physiol., **46**, pp. 599–602.

[27] Kelman, G. R., 1967, "Digital Computer Procedure for Conversion of PcO_2 Into Blood Co_2 Content," Respir. Physiol., **3**, pp. 111.

[28] Weibel, E. R., 1963, *Morphometry of the Human Lung*, Academic, New York, p. 151.

[29] Haefeli-Bleuer, B., and Weibel, E. R., 1988, "Morphometry of the Human Pulmonary Acinus," Anat. Rec., **220**, pp. 401–414.

[30] Hernan, L. J. et al., 1996, "Perfluorocarbon-Associated Gas Exchange in Normal and Acid-Injured Large Sheep," Crit. Care Med., **24**, pp. 475–481.

[31] Overbeck, M. C. et al., 1996, "Efficacy of Perfluorocarbon Partial Liquid Ventilation in a Large Animal Model of Acute Respiratory Failure," Crit. Care Med., **24**, pp. 1208–1214.

[32] Baden, H. P. et al., 1997, "High-Frequency Oscillatory Ventilation With Partial Liquid Ventilation in a Model of Acute Respiratory Failure," Crit. Care Med., **25**, pp. 299–302.

[33] Hoskyns, E. W., Milner, A. D., and Hopkin, I. E., 1992, "Measurement of Tidal Lung Volumes in Neonates During High-Frequency Oscillation," J. Biomed. Eng., **14**, pp. 16–20.

[34] Scalfaro, P. et al., 2001, "Reliable Tidal Volume Estimates at the Airway Opening With an Infant Monitor During High-Frequency Oscillatory Ventilation," Crit. Care Med., **29**, pp. 1925–1930.

[35] Lango, T., Morland, T., and Brubakk, A. O., 1996, "Diffusion Coefficients and Solubility Coefficients for Gases in Biological Fluids and Tissues: A Review," Undersea Hyperbaric Med., **23**, pp. 247–272.

[36] Tham, M. K., Walker, R. D., and Modell, J. H., 1973, "Diffusion-Coefficients of O_2, N_2, and Co_2 in Fluorinated Ethers," J. Chem. Eng. Data, **18**, pp. 411–412.

[37] Paiva, M., 1973, "Gas Transport in Human Lung," J. Appl. Physiol., **35**, pp. 401–410.

[38] Davidson, M. R., and Fitz-Gerald, J. M., 1972, "Flow Patterns in Models of Small Airway Units of Lung," J. Fluid Mech., **52**, p. 161.

[39] Wei, H. H., and Grotberg, J. B., "Flow and Transport in a Rhythmically Breathing Alveolus Partially Filled With Liquid," Phys. Fluids (Submitted).